Intraband and interband optical deformation potentials in femtosecond-laser-excited α-Te

Sergey I. Kudryashov
Department of Physics, Arkansas State University, Arkansas 72467-0419, USA

Maria Kandyla, Christopher A. D. Roeser,* and Eric Mazur
Department of Physics and Division of Engineering and Applied Sciences, Harvard University, 9 Oxford Street, Cambridge, Massachusetts 02138, USA

(Received 21 October 2006; published 13 February 2007)

We calculated the intraband and interband optical deformation potentials for semiconducting α-Te from experimental data of the band gap shrinkage and softening of the A_1-optical phonon mode in response to femtosecond laser excitation. These potentials were obtained by applying first- and second-order perturbation theory to the Frölich Hamiltonian describing the carrier-phonon interaction. The intraband optical deformation potential is considerably smaller than previously estimated values; there are no previously reported values for the interband optical deformation potential.

DOI: 10.1103/PhysRevB.75.085207 PACS number(s): 78.47.+p, 61.80.Ba, 63.20.Kr, 78.20.Bh

I. INTRODUCTION

The development of femtosecond lasers in the early 1980s enabled experimental studies of dynamics of coherent optical phonons driven by electron-hole plasma excitation in semiconductors, semimetals, and metals.[1–5] The resulting subpicosecond oscillations in the crystalline structure modulate the band structure and manifest themselves as quasiperiodic oscillations of the isotropic or the anisotropic optical reflectivity of the absorbing materials at the optical phonon frequency Ω_o.[3,6] The oscillations are superimposed on a background component which includes contributions from the Drude gas, and screening, exchange, and correlation band gap renormalization effects from the photoexcited electron-hole plasma (EHP).[7] The background component also includes a contribution from a quasistatic displacement of the ion sublattice towards a new EHP-defined equilibrium position.[1,6] Surprisingly, this displacement drives the material toward a more symmetric crystalline structure, usually a metallic Peierls phase.[4,8] At high electronic excitation the coherent optical phonons exhibit EHP-induced softening, reducing Ω_o by up to 20%.[3–5]

The EHP-driven excitation and softening of the coherent optical phonons and the phonon-induced band gap shrinkage in many semiconductors and semimetals represent an initial stage of dynamic displacive Peierls (Jahn-Teller) structural distortions caused by deformation-potential electron/hole optical phonon (e,h-phonon) coupling.[8] Such coupling can be characterized by diagonal (intraband) and off-diagonal (interband) matrix elements of the optical deformation potentials. Optical deformation potentials are key parameters for the understanding of electronic transport of "hot" carriers and related lattice phenomena in semiconductors and insulators.[9,10]

Few experimental techniques permit the determination of optical deformation potentials in semiconductors. Examples are Raman scattering and temperature-dependent hole mobility.[10,11] Consequently, for many materials, especially for semimetals and narrow-gap semiconductors with complicated band structures, these potentials are not known and difficult to obtain theoretically. In particular, for crystalline α-Te the only theoretical value for intraband optical deformation potentials (averaged over k space in the first Brillouin zone) was estimated[12] using results of density functional theory (DFT) calculations.[13] In this paper we derive values for the intraband and interband optical deformation potential for tellurium from experimental data of phonon-induced band gap renormalization and EHP-induced phonon softening.

II. THEORY

Deformation-potential e,h-optical phonon interaction is the major cause of Peierls metal-insulator structural distortions[8] because it is less sensitive to EHP screening than the Frölich interaction between charge carriers (electrons and holes) with IR-active phonons,[11] particularly in a strongly correlated state near the metal-insulator transition. Consequently, for EHP densities $N_{e,h} > 10^{21}$ cm^{-3} only zone-center Raman-active A_1—and possibly infrared- and Raman-active $E_{1,2}$ (Ref. 14)—optical phonon modes can be coherently excited in α-Te by ultrashort laser pulses via the deformation potential-like displacive excitation of coherent phonons mechanism.[1] These zone-center phonons have wave vector $\boldsymbol{q}=0$. Because of screening at high EHP densities, impulsive stimulated Raman scattering is not an effective mechanism for generating long-wavelength coherent optical phonons with $\boldsymbol{q}\approx 0$, as required by the energy and momentum conservation rules of the scattering process.[11]

Deformation-potential e,h-phonon coupling is usually described by the Frölich Hamiltonian,[15,16] which, when adapted to describe coherent optical phonons with $\boldsymbol{q}=0$, can be written as

$$H_{\text{Frölich}} = \sum_{\alpha\beta k} \varepsilon_{\alpha\beta k} c^{\dagger}_{\alpha k} c_{\beta k} + N_o h \Omega_o b^{\dagger}_o b_o + \sum_{\alpha\beta k} M_{\alpha\beta k}(b^{\dagger}_o + b_o) c^{\dagger}_{\alpha k} c_{\beta k}, \quad (1)$$

where k is the carrier quasimomentum. The first term in the Frölich Hamiltonian describes the total energy of the electronic subsystem represented by the sum of corresponding

 ©2007 The American Physical Society

diagonal terms with carrier self-energies $\varepsilon_{\alpha\alpha k}$ in band α and electronic band occupation numbers $n_{\alpha k}=c^{\dagger}_{\alpha k}c_{\alpha k}$, where $c^{\dagger}_{\alpha k}$ and $c_{\alpha k}$ are the second-quantization creation and annihilation operators, respectively. The off-diagonal elements represent real or virtual electronic transitions between arbitrary bands α and β, separated by the gap $\varepsilon_{\alpha\beta k}=\varepsilon_{\alpha\alpha k}-\varepsilon_{\beta\beta k}$. The second term describes the total energy of the coherent optical phonons with energy quanta $h\Omega_o$ and phonon second-quantization creation and annihilation operators $b^{\dagger}_o$ and b_o, respectively; N_o is a calibration constant corresponding to the number of primitive unit cells, containing three six-valent Te atoms each, in the excited region of the sample. The third term is the deformation potential Hamiltonian H_{DP}, which represents the carrier-phonon interaction and which is given by the diagonal and off-diagonal e,h-phonon coupling matrix elements $M_{\alpha\beta k}=\sqrt{2}V_{\alpha\beta k}U_o$. The optical deformation potential $V_{\alpha\beta k}$ is a matrix element of the Fourier transform of the screened ion potential arising from the coherent optical phonon lattice displacement; $U_o=[h/(8\pi^2\mu\Omega_o)]^{1/2}$ is the zero-energy phonon oscillation amplitude, $\mu=M/3$ is the reduced mass of the A_1-optical phonon in α-Te, and M is the atomic mass.

The total energy of the electron-phonon system can be written as $E=E_o+E_1+E_2+\cdots$, where the zeroth-order term $E_o=\Sigma\varepsilon_{\alpha\alpha k}n_{\alpha k}+N_o n_o h\Omega_o$ represents the total energy of the noninteracting electrons and phonons, and the E_i are higher-order perturbation terms due to the electron-phonon interactions. The first-order term, due to the deformation potential Hamiltonian, contributes

$$E_1=\langle\ldots,n_{\alpha k},\ldots,n_o+1|H_{DP}|\ldots,n_{\alpha k},\ldots,n_o\rangle = \sqrt{n_o+1}\sum_{\alpha k} M_{\alpha\alpha k}n_{\alpha k}, \quad (2)$$

where the bra and ket state vectors $\langle\ldots,n_{\alpha k},\ldots,n_o+1|$ and $|\ldots,n_{\alpha k},\ldots,n_o\rangle$, are electron and phonon number states with occupation numbers $n_{\alpha k}$ and n_o (or n_o+1), respectively. Differentiating $E=E_o+E_1$ with respect to n_o and setting the derivative equal to zero, we obtain a mechanical stability condition for the ions in the EHP-induced equilibrium positions

$$\sqrt{n_o+1}=-\frac{\sum_{\alpha k} M_{\alpha\alpha k}n_{\alpha k}}{2N_o h\Omega_o}, \quad (3)$$

where the product $\sqrt{2(n_o+1)}U_o$ defines a full oscillation amplitude of the ion sublattice U_{full} which is nearly equal to the quasistatic displacement U_{qs} of the ion sub-lattice to a new EHP-defined equilibrium position.[17] Using Eqs. (2) and (3) we obtain for the renormalization of the carrier self-energies $\Delta\varepsilon_{aak}=(\partial E_1/\partial n_{ak})$ in band α

$$\Delta\varepsilon_{\alpha\alpha k}=M_{\alpha\alpha k}\sqrt{n_o+1}=-\frac{M_{\alpha\alpha k}\sum_{\beta k'} M_{\beta\beta k'}n_{\beta k'}}{2N_o h\Omega_o}. \quad (4)$$

This renormalization results in a band gap change $\Delta\varepsilon_{a\beta k}=\Delta\varepsilon_{aak}-\Delta\varepsilon_{\beta\beta k}$. According to group theory, the interaction between free carriers and the fully symmetrical A_1-phonon mode in α-Te renormalizes all bands in proportion to their diagonal e,h-phonon coupling elements M_{aak} because the direct product of the irreducible representations characterizing these bands Γ_i and the identity irreducible phonon representation A_1 yields $\Gamma_i\otimes A_1=\Gamma_i$. At high carrier densities, $N_{e,h}>10^{21}$ cm^{-3}, another significant band gap renormalization contribution is due to purely electronic screening, exchange, and correlation effects[7] as discussed below.

The second-order contribution to the total energy comes from coherent scattering of carriers by optical phonons to intermediate electronic states and back to their initial electronic states without a change in phonon or electronic occupation numbers.[16] This process results in a change in the phonon frequency Ω_o. For the A_1-phonon mode the second-order contribution to the total energy E of the system is given by[16]

$$E_2=N_o\langle\ldots,n_{\alpha k},\ldots,n_o|H_{DP}|(E_o-H_o)^{-1}|H_{DP}|\ldots,n_{\alpha k},\ldots,n_o\rangle \approx 2n_o\sum_{\alpha\neq\beta,k}\frac{|M_{\alpha\beta k}|^2 n_{\alpha k}}{\varepsilon_{\alpha\beta k}}+\sum_{\alpha\neq\beta,k}\frac{|M_{\alpha\beta k}|^2 n_{\alpha k}(1-n_{\beta k})}{N_o\varepsilon_{\alpha\beta k}}. \quad (5)$$

Differentiating $E=E_o+E_1+E_2$ with respect to n_o and substituting Eqs. (2) and (3) yields the renormalized phonon self-energies

$$h\Omega\approx h\Omega_o+2\sum_{\alpha\neq\beta,k}\frac{|M_{\alpha\beta k}|^2}{\varepsilon_{\alpha\beta k}}\frac{n_{\alpha k}}{N_o}, \quad (6)$$

where transitions $\alpha\rightarrow\beta$ must obey the symmetry selection rule $\Gamma_i\otimes A_1=\Gamma_i$ (see above) and are characterized by a set of nondiagonal e,h-phonon coupling matrix elements $M_{a\beta k}$ which are related to the corresponding nondiagonal (interband) optical deformation potentials. The relative contributions of different transitions also depend strongly on the sign and magnitude of the corresponding band gap $\varepsilon_{\alpha\beta k}$.

Equations (4) and (6) provide analytical expressions for the coherent optical phonon-induced band gap renormalization and phonon softening, respectively. The resulting expressions show how the band gap and phonon frequency change as a function of electronic excitation. By comparing these expressions to experimental data we will obtain values for the intraband and interband optical deformation potentials of α-Te (see Sec. IV).

III. EXPERIMENTAL SETUP AND TECHNIQUE

The response of the dielectric function of α-Te to femtosecond laser photoexcitation has been measured with femtosecond time resolution using a dual-angle-of-incidence pump-probe reflectometry technique.[18] These experiments were performed on a single-crystal Czochralski-grown tellurium sample using 800-nm pulses from a multipass amplified Ti:sapphire laser, producing 0.5-mJ, 35-fs pulses (full width at half maximum) at a repetition rate of 1 kHz.[19] Briefly, an s-polarized excitation pulse ("pump") excites the sample at different absorbed peak laser fluences F_{abs} below the threshold for permanent visible damage $F_{\text{th}}=2.1$ mJ/cm^2, while the transient reflectivity is measured using a p-polarized white-light pulse ("probe"; $\hbar\omega=1.65-3.2$ eV). Two-photon absorption measurements[20] show that the time resolution of

the pump-probe setup is better than 50 fs, while calculations based on measurements of the spectrum and chirp of the white-light probe indicate that the time resolution of the probe varies from 20 fs near 1.7 eV to 60 fs near 3.2 eV.[21] The entire system is calibrated to obtain absolute reflectivity.

The optic axis c of the tellurium sample lies in the plane of the sample surface, perpendicular to the plane of incidence of the probe. To measure the ordinary dielectric function $\varepsilon_{\mathrm{ord}}(\omega)$, the sample is oriented such that the electric field of the excitation pulse $E_{\mathrm{exc}} \| c$ ("ordinary probe geometry"). The ordinary dielectric function $\varepsilon_{\mathrm{ord}}(\omega)$ can then be determined from spectral reflectivity measurements at two angles of incidence (68.4° and 80.4°).[3] Measurements at the same two angles of incidence with the sample rotated so that $E_{\mathrm{exc}} \perp c$ ("extraordinary probe geometry"), allow determination of values for the extraordinary dielectric function $\varepsilon_{\mathrm{ext}}(\omega)$, given measured values of $\varepsilon_{\mathrm{ord}}(\omega)$ at each corresponding time delay. For negative time delays, when the probe arrives before the excitation pulse, the experimentally determined $\varepsilon_{\mathrm{ord}}(\omega)$ and $\varepsilon_{\mathrm{ext}}(\omega)$ are in excellent agreement with corresponding literature data for (unexcited) tellurium.[22] Further details on the experimental technique can be found in Refs. 3 and 18.

The dynamics of the experimentally measured dielectric functions are analyzed by a fit of a Drude-Lorentz model[23] to the data at each time delay. The Drude-Lorentz model for a single oscillator can be written as

$$\varepsilon(\omega) = \frac{Ne^2}{\varepsilon_{\mathrm{o}} m} \frac{1}{\omega_{\mathrm{res}}^2 - \omega^2 - i\omega\Gamma}, \tag{7}$$

where the free parameters are the resonance energy $E_{\mathrm{res}} = \hbar\omega_{\mathrm{res}}$, the resonance linewidth $\hbar\Gamma$, and the oscillator strength $f = Ne^2/\varepsilon_{\mathrm{o}} m$. While the imaginary parts of the dielectric functions of tellurium are well-fit by this model, resonances outside the spectral range of the probe give roughly constant contributions to the real part of the dielectric function within the probe range, so a real additive constant C was included in the fit to $\varepsilon_{\mathrm{ord}}(\omega)$ and $\varepsilon_{\mathrm{ext}}(\omega)$ to account for this effect. The resonance energies from a fit of literature values for $\varepsilon_{\mathrm{ord}}(\omega)$ and $\varepsilon_{\mathrm{ext}}(\omega)$ over the spectral range of the probe pulse are $E_{\mathrm{res,ord}} \approx 2.3$ eV and $E_{\mathrm{res,ext}} \approx 2.1$ eV.

Figure 1 shows the transient behavior of the resonance energies $E_{\mathrm{res,ord}}$ and $E_{\mathrm{res,ext}}$ at $F_{\mathrm{abs}} = 0.85 F_{\mathrm{th}}$. Because of a transient band gap renormalization each resonance energy redshifts by an amount $\Delta E_{\mathrm{res}}(t) = [E_{\mathrm{res}}(t<0) - E_{\mathrm{res}}(t)]$ reaching a maximum at a time delay of 0.1–0.3 ps and oscillating at a time- and fluence-dependent frequency $\Omega < \Omega_{\mathrm{o}}$, where $\Omega_{\mathrm{o}} \approx 3.6$ THz is the A_1-phonon frequency in α-Te at 295 K.[24] The time-dependent frequency Ω can be determined from the oscillations in Fig. 1 for the time interval $\Delta t \approx 0.3$–2 ps; from these data we extrapolated values of Ω_{ord} and Ω_{ext} at $\Delta t = 0.1$ ps, when we expect the carrier density to reach its maximum value. The fluence dependence of these $\Omega_{\mathrm{ord,ext}}(\Delta t \approx 0.1 \text{ ps})$ frequencies shows the softening[2] of the A_1-mode as the excitation increases (Fig. 2).

The maximum negative band gap renormalization (redshift) of the resonance energies $|\Delta E_{\mathrm{res,max}}|$, which is reached for time delays $\Delta t \approx 0.1$–0.3 ps, consists of two nonthermal

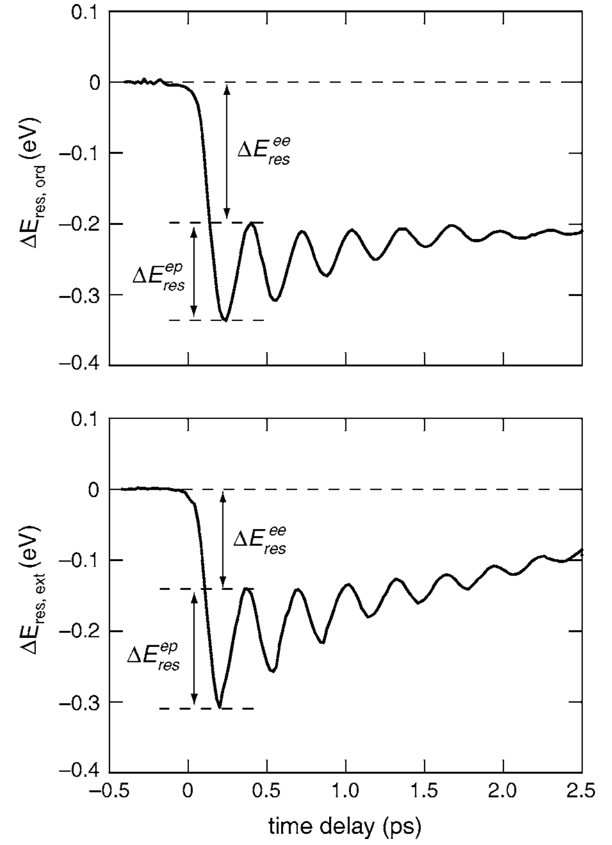

FIG. 1. Transient shifts of the resonance energy E_{res} of the ordinary (top) and extraordinary (bottom) dielectric functions of α-Te at absorbed laser fluence $F_{\mathrm{abs}} = 0.85 F_{\mathrm{th}}$. The shifts have an electronic component ($\Delta E_{\mathrm{res}}^{ee}$) and a phonon-induced component ($\Delta E_{\mathrm{res}}^{ep}$).

contributions. One is purely electronic and consists of screening, exchange, and correlation effects in the electron-hole plasma. The other contribution is due to the deformation-potential e,h-optical phonon interaction. We will denote the electronic part by $\Delta E_{\mathrm{res}}^{ee}$ and the phonon part

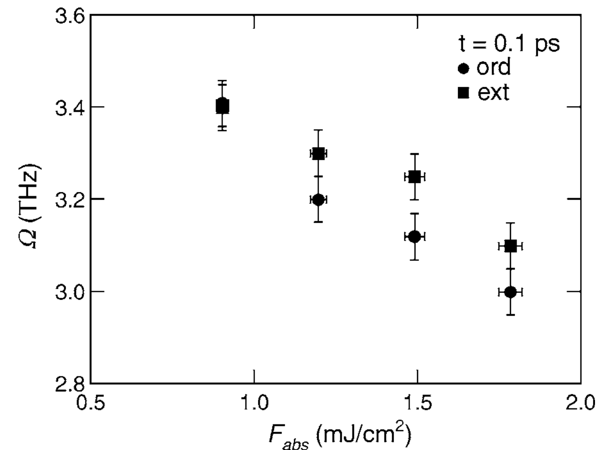

FIG. 2. Fluence dependence of the A_1-phonon oscillation frequency Ω in α-Te, obtained by Fourier transforming (Ref. 12) the transient shifts in resonance energy of the ordinary (circles) and extraordinary (squares) dielectric functions of α-Te, evaluated around $t \approx 0.1$ ps.

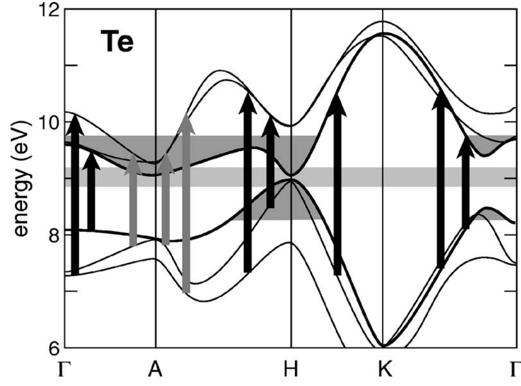

FIG. 3. Renormalized band structure of the VB3 and CB1 bands for α-Te (after Refs. 13 and 24). The regions probed in the ordinary probe geometry are marked by grey arrows; the length of the arrows corresponds to the range of probe frequencies used (1.65–3.2 eV). The regions probed in the extraordinary geometry are marked by black arrows. The grey shading in the valleys shows the free carrier population in the conduction and valence bands at maximum $k_BT_{e,h}\approx 0.28$ eV. The light grey horizontal band shows the initial H-point direct band gap of 0.33 eV.

by $\Delta E_{\mathrm{res}}^{ep}$. Because the excitation pulses are much shorter than the phonon period ($\tau_{\mathrm{exc}}\approx 35$ fs and $T_{\mathrm{ph}}\approx 0.3-0.4$ ps, respectively) the amplitude of the oscillations of the ions around their displaced equilibrium positions is equal to their quasistatic displacement: $U_{\mathrm{qs}}=U_{\mathrm{osc}}$ (Ref. 15) and the total phonon displacement is $U(t)=U_{\mathrm{qs}}(t)+\mathrm{U}_{\mathrm{osc}}(t)$. According to Eq. (3) the quasistatic phonon-induced component $\Delta E_{\mathrm{res}}^{\mathrm{qs}}$ is thus equal to the amplitude of the oscillating part $\Delta E_{\mathrm{res}}^{\mathrm{osc}}(t)$, and so

$$\Delta E_{\mathrm{res}}^{ep}(t) = \Delta E_{\mathrm{res}}^{\mathrm{qs}}(t) + \Delta E_{\mathrm{res}}^{\mathrm{osc}}(t) = 2\Delta E_{\mathrm{res}}^{\mathrm{qs}}(t). \tag{8}$$

The pedestals in the $\Delta E_{\mathrm{res}}(t)$ curves in Fig. 1 are due to the fast electronic component $\Delta E_{\mathrm{res}}^{ee}(t)$. We estimate that the timescale for this electronic response is on the order of 50 fs and therefore its contribution to the slope of the initial, monotonically decreasing part of the $\Delta E_{\mathrm{res}}(t)$ curve, blends together with the lattice response producing a smooth, single-time-scale shape. This separation of ΔE_{res} into electronic and phonon components is supported by recent theoretical results[7] and shows the importance of both electronic and phonon contributions during band gap collapse in semiconductors.

For the complex structure of the top valence band (VB3 or p-lone pair) and the bottom conduction band (CB1 or p antibonding) of α-Te (see Fig. 3 and Ref. 24) $\Delta E_{\mathrm{res}}^{ee}$ and $\Delta E_{\mathrm{res}}^{ep}$ represent averages of individual band gap renormalization subband shifts over the three VB3 and CB1 subbands and over k space. As a result, we have

$$\Delta E_{\mathrm{res}}^{ep} = \sum\nolimits_{k'} [\Delta E_{\mathrm{VB3},k'}^{ep} + \Delta E_{\mathrm{CB1},k'}^{ep}] = \sum\nolimits_{k'} [V_{\mathrm{VB3},k'} + V_{\mathrm{CB1},k'}] \times (U_{\mathrm{qs}} + U_{\mathrm{osc}}) = V_{C/V,k'}(U_{\mathrm{qs}} + U_{\mathrm{osc}}) \tag{9}$$

and

$$\Delta E_{\mathrm{res}}^{ee} = \sum\nolimits_{k'} [\Delta E_{\mathrm{VB3},k'}^{ee} + \Delta E_{\mathrm{CB1},k'}^{ee}], \tag{10}$$

where the k' label the regions of the k-space that are sampled in the ordinary and extraordinary probe geometries, while $V_{\mathrm{VB3},k'}$, $V_{\mathrm{CB1},k'}$, and $V_{C/V,k'}$ correspond to the average valence band, conduction band, and overall intraband optical deformation potentials, respectively. The grey and black arrows in Fig. 3 show the regions that are sampled by the probe continuum. In the extraordinary probe geometry, selection rules limit the probing to the region near the A-point (grey arrows), while in the ordinary probe geometry, states near the Γ, H, K, and M points are probed (black arrows).

IV. ANALYSIS OF EXPERIMENTAL RESULTS

A. Determination of EHP density

In Sec. II we derived expressions for the band gap renormalization and phonon softening as a function of the electronic occupation number $n_{\alpha k}$, which is directly related to the EHP density $N_{e,h}$ [Eqs. (4) and (6)]. In order to provide a quantitative interpretation of the experimental data presented in the previous section and to determine the intraband and interband optical deformation potentials in α-Te, we need to calculate the EHP density $N_{e,h}$ near the sample surface as a function of F_{abs}. Because the photon energy in the excitation beam (1.55 eV) greatly exceeds the minimum band gap in α-Te [$E_{g,H}\approx 0.33$ eV Ref. 24], the excitation pulse produces "hot" holes and electrons in the VB3 and CB1 bands, respectively. Two-particle impact ionization causes the photoexcited carriers within each band to relax on the femtosecond scale, a rate that is comparable to that of the energy relaxation and thermalization in an electron-hole plasma via screened Coulomb carrier-carrier (e,h-e,h) interactions.[25] The reverse process, Auger recombination, occurs on a much slower, sub-ps time scale at the moderate $N_{e,h}/N_v$ ratios achieved in this study, where $N_v=1.8\times 10^{23}$ cm^{-3} is the total density of valence electrons in α-Te. The ultrafast shrinking of the band gap observed in α-Te after the arrival of the excitation pulse (see Fig. 1), further increases the role of impact ionization. As a result, electrons and holes reach a common EHP temperature $T_{e,h}$ during the excitation pulse, populating the renormalized minimum and maximum of the conduction and valence bands at the A and H points, respectively (see Fig. 3).

We can calculate the EHP density $N_{e,h}$ generated by linear absorption of a pulse with a given absorbed fluence F_{abs} from the following energy and particle number balance equations.

$$E_{\mathrm{abs}}(F_{\mathrm{abs}}) = \frac{F_{\mathrm{abs}}}{\delta_{\mathrm{exc}}^{*}} = \int_{-\infty}^{\mu} \varepsilon D_h(\varepsilon) f_{\mathrm{FD}}(\varepsilon, T_{e,h}) d\varepsilon + \int_{\mu}^{+\infty} \varepsilon D_e(\varepsilon) f_{\mathrm{FD}}(\varepsilon, T_{e,h}) d\varepsilon, \tag{11}$$

$$N_{e,h}(F_{abs}) = \int_{-\infty}^{\mu} D_h(\varepsilon) f_{\mathrm{FD}}(\varepsilon, T_{e,h}) d\varepsilon = \int_{\mu}^{+\infty} D_e(\varepsilon) f_{\mathrm{FD}}(\varepsilon, T_{e,h}) d\varepsilon, \tag{12}$$

where $E_{\rm abs}$ is the absorbed volume energy density, $D_{e,h}(\varepsilon)$ are the electron (hole) density-of-states distributions at carrier self-energies ε above (below) the Fermi level μ, $f_{\rm FD}(\varepsilon,T_{e,h})$ is the Fermi-Dirac distribution of carriers in the corresponding bands, and $\delta^*_{\rm exc}=\delta_{\rm exc}+\delta_{\rm dif}$ is the effective energy deposition depth which is determined by the absorption depth $\delta_{\rm exc}$ of the excitation pulse and the EHP ambipolar diffusion depth $\delta_{\rm dif}\approx(D_{\rm dif}t)^{1/2}$ with $D_{\rm dif}$ the diffusion coefficient.

Because the excitation and probe beams are orthogonally polarized, the electric field vector of the excitation pulse is perpendicular to the c-axis ($E_{\rm exc}\perp c$) in the extraordinary probe geometry and so the (ordinary) index of refraction at the excitation wavelength is $n_{\rm exc}=n_{\rm ord}$ (800 nm)$=5.84+1.06i$ (Ref. 22) yielding a penetration depth for the excitation field of $\delta_{\rm pu}$(800 nm)≈ 60 nm. Using a carrier diffusion coefficient $D_{\rm dif}=6-40{\rm cm}^2/{\rm s}$,[2,13] we obtain a diffusion length of $\delta_{\rm dif}\approx 10-30$ nm over the time interval $\Delta t\approx 0.1-0.3$ ps, which is smaller than the penetration depth of the excitation pulse and so $\delta^*_{\rm exc}\approx\delta_{\rm exc}$. At the $E_{\rm res,ext}$ peak wavelength λ(2.1 eV)$\approx$600 nm the index of refraction is $n_{\rm pr}=n_{\rm ext}$ (600 nm)$=5.76+4.92i$ (Ref. 22) giving an effective probe depth $\delta^*_{\rm pr}\approx\delta_{\rm pr}$ (600 nm)$\approx$10 nm. Therefore $\delta^*_{\rm exc}\gg\{\delta_{\rm dif},\delta^*_{\rm pr}\}$, which ensures that we are probing a nearly homogeneously excited region near the surface of the α-Te.

Using a numerical fitting procedure we fitted Eq. (11) to the experimental values of $E_{\rm abs}(F_{\rm abs})$ and the known values for $\delta_{\rm exc}$ with $T_{e,h}$ as a free parameter. For the nearly symmetrical electronic density of states distribution [constant $D_{e,h}(\varepsilon)=0$ at $|\varepsilon|\leqslant E_{g,H}/2$ and linearly increasing $D_{e,h}(\varepsilon)\approx 5\times 10^{22}$ ε states/(eV^2 cm^3) at $E_{g,H}/2\leqslant|\varepsilon|\leqslant 1$ eV (Refs. 24 and 26)], the Fermi level μ can be chosen exactly in the middle of the H-point band gap $E_{g,H}\approx 0.33$ eV. We further assume that the maximum nonthermal, electronic and coherent optical phonon-induced band gap renormalization for the VB3 and CB1 bands symmetrically shrinks the band gap at the H point. Because the band gap renormalization is approximately equal to $|\Delta E^{ee}_{\rm res}|+|\Delta E^{ep}_{\rm res}|$, both the electron and hole density of states distributions are shifted towards the Fermi level by an amount equal to $[|\Delta E^{ee}_{\rm res}|+|\Delta E^{ep}_{\rm res}|]/2$. Figure 4(a) shows the values obtained from the fitting for $k_BT_{e,h}$ as a function of the absorbed fluence $F_{\rm abs}$ in the extraordinary probe geometry.

The values of $k_BT_{e,h}$ in Fig. 4(a) range from 0.2 to 0.3 eV and represent an upper limit for the thermal energy of the carriers due to impact ionization $k_BT_{e,h}\approx\frac{1}{2}(E_{g,H}-|\Delta E^{ee}_{\rm res,ext}|-|\Delta E^{ep}_{\rm res,ext}|)+\varepsilon^{eff}_{e,h}$, where the $\varepsilon^{eff}_{e,h}$ are the $N_{e,h}$-dependent dynamic Burnstein-Moss (band filling) energy shifts in the conduction and valence bands, respectively.[27] The $k_BT_{e,h}$ values we obtain differ from the 0.05-eV value used in Ref. 13. The range of values we find for $k_BT_{e,h}$ indicate that almost 90% of the excited carriers occupy an energy interval of 0.5–0.7 eV near the edges of CV1 and VB3 bands, predominantly near the main high-symmetry points (Γ,A,H) of the first Brillouin zone (see Fig. 3).

We can now determine the electron-hole plasma density $N_{e,h}$ by substituting values for $k_BT_{e,h}$ from Fig. 4(a) into Eq. (12). The square symbols in Fig. 4(b) show the resulting fluence dependence of the EHP density. The relation between EHP density and fluence in Fig. 4(b) allows us to obtain the EHP density dependence of Ω from the data (squares) shown in Fig. 2. The result, shown in Fig. 5 as square symbols, reveals a linear dependence of Ω on EHP density, in agree-

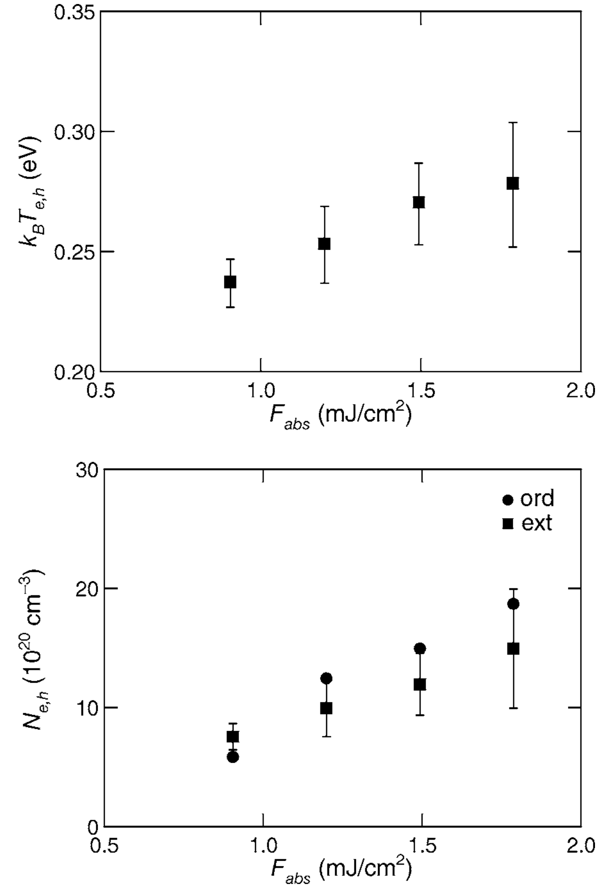

FIG. 4. Fluence dependence of (a) the calculated carrier thermal energy $k_BT_{e,h}$ in the ordinary excitation geometry and (b) the electron-hole plasma density $N_{e,h}$ in both the ordinary and extraordinary excitation geometries.

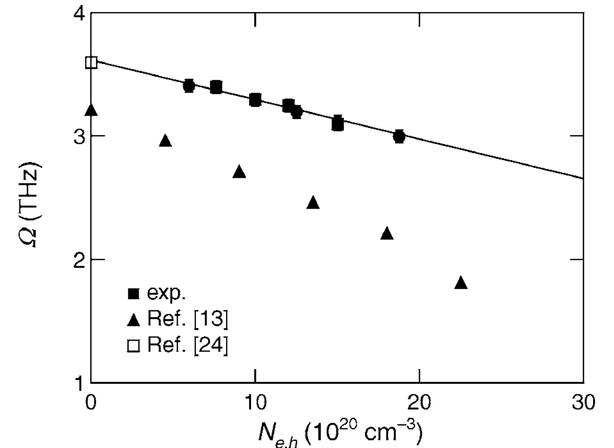

FIG. 5. Dependence of the resonance frequency Ω of the ordinary (circles) and extraordinary (squares) dielectric functions on the electron-hole plasma density. The triangles represent theoretical data obtained from Ref. 13. The value for Ω_o for unexcited α-Te is taken from Ref. 24.

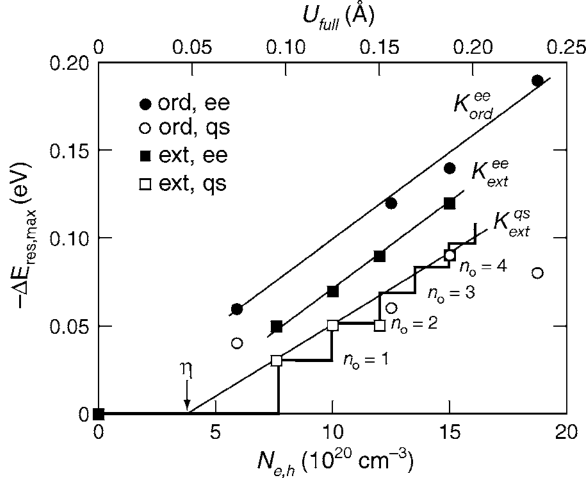

FIG. 6. Dependence of the transient dielectric function resonance shifts $|\Delta E^{ee}_{\text{res,ext}}|$ (solid squares), $|\Delta E^{ee}_{\text{res,ord}}|$ (solid circles), $|\Delta E^{qs}_{\text{res,ext}}|$ (open squares) and $|\Delta E^{qs}_{\text{res,ord}}|$ (open circles) on the electron-hole plasma density $N_{e,h}$ (bottom axis) and on the phonon amplitude U_{full} (top axis). The steplike curve represents a fit of $\Delta E_{\text{res},k\approx A}(U_{\text{full}})$ to the $|\Delta E^{qs}_{\text{res,ext}}|$ data.

ment with Eq. (6). The data in Fig. 5 also agree qualitatively with the results from density functional theory calculations.[13]

In the ordinary probe geometry we cannot use the same approach to determine values for $k_BT_{e,h}$ and $N_{e,h}$ because significant ambipolar diffusion occurs in this configuration: $\delta_{\text{dif}} \approx 10-30$ nm for $D_{\text{dif}}=6-40$ cm^2/s (Refs. 2 and 13) and $\Delta t \approx (0.1-0.3$ ps) on an initial steep Beer's distribution of E_{abs} characterized by $\delta_{\text{exc}}(800\text{ nm}) \approx 22$ nm for $n_{\text{exc}} = n_{\text{ext}}(800\text{ nm}) = 6.73+2.89i$.[22] Figure 2, however, shows that excitation by "ordinary" ($\delta_{\text{exc}} \approx 60$ nm) and "extraordinary" ($\delta_{\text{exc}} \approx 20$ nm) excitation pulses results in similar values of Ω, which leads us to conclude that the EHP densities are also quite similar in both geometries. Therefore, we can use the dependence of Ω on $N_{e,h}$ from Fig. 5 to determine the EHP densities for the Ω_{ord} data obtained in the ordinary probe geometry (circles in Fig. 2). The circles in Fig. 4(b) show the resulting dependence of $N_{e,h}$ on F_{abs} in the ordinary probe geometry.

B. Determination of intraband and interband optical deformation potentials

The measured transient shifts $\Delta E_{\text{res,ext}}(t)$ of the resonance energy of the imaginary part of the extraordinary dielectric function (Fig. 1) reveal the time-dependent band gap renormalization between the CV1 and VB3 bands around the A point in the α-Te band structure (grey arrows in Fig. 3). In Fig. 6 we plot the maximum values of these transient shifts as a function of the EHP density $N_{e,h}$. We can separate these transient shifts into an electronic component $|\Delta E^{ee}_{\text{res,ext}}|$ and a quasistatic phonon component $|\Delta E^{\text{qs}}_{\text{res,ext}}|$, as given by Eq. (8). The resulting range of values for $|\Delta E^{ee}_{\text{res,ext}}|$ (0.05–0.12 eV) for EHP densities in the range 7×10^{20} cm^{-3} to 15×10^{20} cm^{-3} is in agreement with theoretical calculations of electronic band gap renormalization in GaAs and Si, which show that $\Delta E^{ee}_g \approx 0.1$ eV for $N_{e,h} \approx 10^{21}$ cm^{-3}.[7] These calculations also predict that the EHP-driven band gap renormalization for photoexcited GaAs should depend linearly on $N_{e,h}$ at $N_{e,h} \geqslant 10^{21}$ cm^{-3}.[7] As can be seen in Fig. 6, our data for $|\Delta E^{ee}_{\text{res,ext}}(N_{e,h})|$ indeed depend linearly on the EHP density with a slope $K^{ee}_{\text{ext}}=[0.95\pm0.03]\times10^{-22}$ eV cm^3. The value of this slope indicates that when 5% of the valence electrons in α-Te are excited ($N_{e,h} \approx 10^{22}$ cm^{-3}), the average VB3-CB1 direct band gap at the A point only shrinks by about 50% (cf. $|\Delta E^{ee}_{\text{res,ext}}(10^{22}\text{ cm}^{-3})| \approx 1$ eV vs $\langle E_{g,k\cong A}\rangle \approx E_{\text{res,ext}} \approx 2$ eV). A similar partial shrinkage due to electronic screening, exchange and correlation effects is expected for GaAs.[7]

The measured transient shifts $\Delta E_{\text{res,ord}}(t)$ of the resonance energy of the imaginary part of the ordinary dielectric function (Fig. 1) reveal the time-dependent band gap renormalization averaged over the entire k space of the first Brillouin zone of α-Te, excluding the region just adjacent to the A point (Fig. 3). When we plot the maximum value of the electronic component of these shifts $|\Delta E^{ee}_{\text{res,ord}}|$ as a function of the EHP density $N_{e,h}$ (Fig. 6), we obtain a line with a slope $K^{ee}_{\text{ord}}=[0.99\pm0.03]\times10^{-22}$ eV cm^3, which is close to the slope K^{ee}_{ext}. Therefore, we conclude that (i) in agreement with theoretical results for GaAs and Si (Ref. 7) the electronic band gap renormalization in α-Te is nearly isotropic and homogeneous due to the high site symmetry of carrier-carrier interactions and (ii) the procedure we used in Sec. IV A to determine the electron-hole plasma density $N_{e,h}$ in the ordinary probe geometry is justified. Most importantly, the values for $|\Delta E^{ee}_{\text{res,ext}}(N_{e,h})|$ and $|\Delta E^{ee}_{\text{res,ord}}(N_{e,h})|$ in Fig. 6 represent experimental data on dynamic electronic band gap renormalization in a semiconductor.

The quasistatic phonon component of $|\Delta E_{\text{res,ext}}|$ (open squares in Fig. 6) exhibits a nearly linear increase with $N_{e,h}$, in agreement with Eq. (4). Its slope, $K^{\text{qs}}_{\text{ext}}=[0.8\pm0.1]\times10^{-22}$ eV cm^3, is very similar to K^{ee}_{ext}, which shows that e,h-phonon contributions to the band gap renormalization around the A point in the α-Te band structure are important. This $K^{\text{qs}}_{\text{ext}}$ value indicates that for the electron-hole plasma density $N_{e,h} \approx 10^{22}$ cm^{-3} discussed above (5% of the valence electrons), coherent optical phonons provide the other 50% shrinking of the average A-point direct VB3-CB1 band gap. Together, the phonon and the electronic contributions induce a total collapse of the band gap and an insulator-metal transition. The excitation threshold we obtain for an insulator-metal transition in Te at the A point of the band structure $N_{BG,k\approx A} \approx 0.05\ N_v$, is close to the theoretically predicted value (0.1 N_v) for lattice instability and metallization thresholds in other semiconductors.[28]

When we fit the $|\Delta E^{\text{qs}}_{\text{res,ext}}(N_{e,h})|$ data to a straight line we observe that the fitting line does not pass through the origin of the axes (Fig. 6). Indeed the point $|\Delta E^{\text{qs}}_{\text{res,ext}}(N_{e,h})|=0$ has a large horizontal offset from the origin, $\eta \approx 3\times10^{20}$ cm^{-3}. Conversely, the point $|\Delta E^{\text{qs}}_{\text{res,ext}}(0)|$ exhibits a large vertical offset of -0.03 eV, which is comparable to the vertical spacing between the $|\Delta E^{\text{qs}}_{\text{res,ext}}|$ data points (open squares). According to Eq. (3), both of these offsets may be explained by taking into account the quantization of $|\Delta E^{\text{qs}}_{\text{res,ext}}|$. Indeed, at small phonon numbers n_o both the quasistatic displacement and the amplitude of the coherent optical phonon $|U_{\text{qs}}(n_o)|$

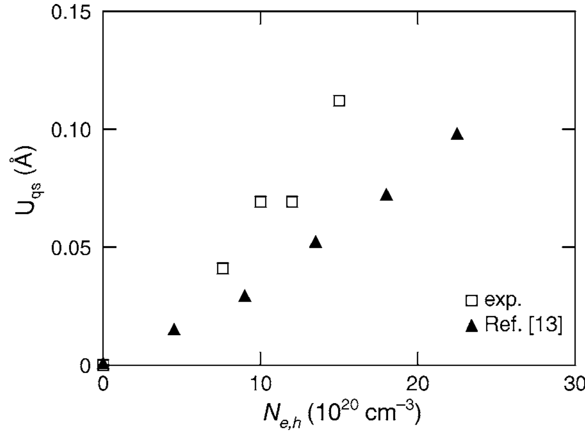

FIG. 7. Dependence of the sublattice phonon displacement U_{qs} on the electron-hole plasma density $N_{e,h}$. The open squares represent the data obtained in this paper; the closed triangles are from Ref. 13.

$=|U_{\mathrm{osc}}(n_o)|\approx(2n_o)^{1/2}U_o$ exhibit quantum character when they are described in the "shifted oscillator" approximation at $\tau_{pu}/T_{ph}\ll 1$.[15] Therefore the electron-hole plasma density $N_{n_o=1}=\eta$ corresponds to the threshold value for EHP-driven emission of the first coherent A_1-optical phonon. The offset disappears when the $|\Delta E^{\mathrm{qs}}_{\mathrm{res,ext}}|$ data are plotted vs. the full oscillation amplitude $U_{\mathrm{full}}=(2n_o+1)^{1/2}U_o$, which includes the zero-energy oscillation amplitude U_o in α-Te (top axis in Fig. 6), and fitted by a steplike function $\Delta E^{\mathrm{qs}}_{\mathrm{res,ext}}(U_{\mathrm{full}})=\Delta E^{\mathrm{qs}}_{\mathrm{res},k\cong A}(U_{\mathrm{full}})=(|V_{C,k\cong A}|+|V_{V,k\cong A}|)[U_{\mathrm{full}}-U_{\mathrm{o}}]$. The difference $[U_{\mathrm{full}}-U_o]$ is equal to $U_{\mathrm{qs}}(n_o)=U_{\mathrm{osc}}(n_o)$ and by definition the deformation-potential e,h-phonon interaction is absent at $n_o=0$. The slope of the step function represents a modulus of the "effective" CB1/VB3 intraband optical deformation potential $|V_{C/V,k\approx A}|=|V_{\mathrm{CB1},k\approx A}|+|V_{\mathrm{VB3},k\approx A}|$. Its value of 0.7 ± 0.1 eV/Å is equal to the average of the A-point intraband optical deformation potentials of the CB1 and VB3 subbands that are sampled by the optical probe.

Likewise, one can represent the data $|\Delta E^{\mathrm{qs}}_{\mathrm{res,ord}}|$ (open circles in Fig. 6) in the form $\Delta E^{\mathrm{qs}}_{\mathrm{res,ord}}(U_{\mathrm{full}})=\Delta E^{\mathrm{qs}}_{\mathrm{res},k-A}(U_{\mathrm{full}})=(|V_{C,k-A}|+|V_{V,k-A}|)[U_{\mathrm{full}}-U_{\mathrm{o}}]$, where the slope $|V_{C/V,k-A}|=|V_{\mathrm{CB1},k-A}|+|V_{\mathrm{VB3},k-A}|$ corresponds to the "effective" CB1/VB3 intraband optical deformation potential and represents electronic states over the entire k space, excluding the A-point region which is not probed optically. The value of the slope $|V_{C/V,k-A}|=0.5\pm0.2$ eV/Å, is somewhat smaller than $|V_{C/V,k\approx A}|=0.7\pm0.1$ eV/Å. Also, the slope of the $|\Delta E^{\mathrm{qs}}_{\mathrm{res,ord}}(N_{e,h})|$ curve $(0.6\pm0.2)\times10^{-22}$ eV cm^3 (not shown in Fig. 6) indicates that the total collapse of the average direct VB3-CB1 band gap $\langle E_{g,k-A}\rangle\approx E_{\mathrm{res,ord}}$ takes place at $N_{BG,k-A}\approx1.4\times10^{22}$ cm^{-3}, i.e., at an EHP density of approximately 0.07 N_v, including both the electronic and phonon-induced band gap renormalization effects.

From the experimental data for $|\Delta E^{\mathrm{qs}}_{\mathrm{res,ext}}|$ in Fig. 6 we can obtain data for $U_{\mathrm{qs}}(N_{e,h})=|\Delta E^{\mathrm{qs}}_{\mathrm{res,ext}}(N_{e,h})|/|V_{C/V,k\approx A}|$ (see Fig. 7). The dependence of U_{qs} on $N_{e,h}$, $U_{\mathrm{qs}}(N_{e,h})\approx[2n_o(N_{e,h})]^{1/2}U_o$, can be described in terms of deformation potentials, by dividing the number of carriers Σn_α and the number of primitive unit cells N_o in Eq. (3) by the volume V_{exc} of the excited material region. Because each primitive unit cell contains three six-valent Te atoms, the volume density of cells in α-Te is $\frac{N_o}{V_{\mathrm{exc}}}=\frac{N_V}{18}$, and $\frac{\Sigma n_a}{V_{\mathrm{exc}}}=N_e+N_h=2N_{e,h}$. Substituting these expressions and $M_{\alpha\beta k}=\sqrt{2}V_{\alpha\beta k}U_{\mathrm{o}}$ into Eq. (3) yields

$$U_{\mathrm{qs}}(N_{e,h})\approx U_{\mathrm{o}}^2\frac{(|V_{\mathrm{CB1},k}|+|V_{\mathrm{VB3},k}|)}{h\Omega(N_{e,h})}\frac{18N_{e,h}}{N_v}. \quad (13)$$

To further simplify this expression we can set the sum of the moduli of the intraband optical deformation potential $|V_{\mathrm{CB1},k}|$ and $|V_{\mathrm{VB3},k}|$ equal to the modulus of an "effective" CB1/VB3 intraband optical deformation potential $|V_{C/V,k}|=|V_{\mathrm{CB1},k}|+|V_{\mathrm{VB3},k}|$. The $U_{\mathrm{qs}}(N_{e,h})$ data in Fig. 7 thus allow us to obtain this deformation potential for the photoexcited carriers that occupy near-edge subbands of the CB1 and VB3 bands (Fig. 3) and that drive the coherent optical phonon displacement $U=U_{\mathrm{osc}}+U_{\mathrm{qs}}$. The $|V_{C/V,k}|$ value obtained from the data in Figs. 5 and 7 using Eq. (13), is equal to 2.2 ± 0.3 eV/Å, considerably exceeding the values we found for $|V_{C/V,k-A}|$ and $|V_{C/V,k\cong A}|$ (0.5 ± 0.2 and 0.7 ± 0.1 eV/Å, respectively).

As predicted by Eq. (6), the $\Omega_{\mathrm{ext}}(N_{e,h})$ and $\Omega_{\mathrm{ord}}(N_{e,h})$ data shown in Fig. 5 exhibit a linear dependence on electronic excitation with a slope $K_{\Omega,\mathrm{exp}}\approx-(3.2\pm0.3)\times10^{-22}$ THz cm^3. This slope is nearly two times smaller than theoretically predicted.[13] When we extrapolate the $\Omega(N_{e,h})$ data to $\Omega(N_{\mathrm{soft}})=0$ we estimate a threshold EHP density for complete softening of the A_1-phonon mode of $N_{\mathrm{soft,exp}}\approx1.1\times10^{22}$ cm^{-3} (0.06 N_v). This value is significantly lower than the threshold of 3.6×10^{22} cm^{-3} (0.19 N_v) calculated in Ref. 2 accounting only for linear photoexcitation of carriers. However, even though $N_{\mathrm{soft,exp}}$ is being determined by a considerable extrapolation of the experimental data, its value is consistent with the average band gap renormalization thresholds, $N_{\mathrm{BG},k\approx A}\approx1.0\times10^{22}$ cm^{-3} and $N_{\mathrm{BG},k-A}\approx1.4\times10^{22}$ cm^{-3} (0.05 and 0.07 N_v, respectively) we determined earlier. Thus, we estimate that the Peierls-like insulator-metal transition in α-Te occurs at the same electronic excitation level as the complete softening of the A_1-phonon mode.

We can obtain interband optical deformation potentials in α-Te from the $\Omega_{\mathrm{ext}}(N_{e,h})$ and $\Omega_{\mathrm{ord}}(N_{e,h})$ data in Fig. 5 by rewriting Eq. (6) as

$$\Omega_{\mathrm{o}}-\Omega(N_{e,h})\approx\frac{4}{h}U_{\mathrm{o}}^2\left[\frac{|V_{\mathrm{CB1,2}}|^2}{\varepsilon_{\mathrm{CB2}}-\varepsilon_{\mathrm{CB1}}}+\frac{|V_{\mathrm{VB2,3}}|^2}{\varepsilon_{\mathrm{VB3}}-\varepsilon_{VB2}}\right]\frac{18N_{e,h}}{N}. \quad (14)$$

In deriving Eq. (14) only virtual CB1↔CB2 [average band gap $\langle|\varepsilon_{\mathrm{CB2}}-\varepsilon_{\mathrm{CB1}}|\rangle\approx5$ eV (Ref. 24)] and VB3↔VB2 [average band gap $\langle|\varepsilon_{\mathrm{VB3}}-\varepsilon_{\mathrm{VB2}}|\rangle\approx3$ eV (Ref. 24)] transitions were taken into account because these are the only allowed transitions by the selection rule $\Gamma_i\otimes A_1=\Gamma_i$; virtual CB1↔VB3 and VB3↔CB1 [average band gap $\langle|\varepsilon_{\mathrm{CB1}}-\varepsilon_{\mathrm{VB3}}|\rangle\approx1.5$ eV (Ref. 24)] transitions of carriers to their initial (unexcited) states and back were neglected to reduce the number of unknown interband optical deformation potentials. Taking an average value of $(\langle|\varepsilon_{\mathrm{CB2}}-\varepsilon_{\mathrm{CB1}}|\rangle+\langle|\varepsilon_{\mathrm{VB3}}-\varepsilon_{\mathrm{VB2}}|\rangle)/2\approx4$ eV in Eq. (14), we obtain an approximate value of about 1.3 eV/Å for each of the interband optical

deformation potentials $|V_{\text{CB1,2}}|$ and $|V_{\text{VB2,3}}|$. If we include the stabilizing effect of virtual lower-energy CB1↔VB3 and VB3↔CB1 transitions, the values for $|V_{\text{CB1,2}}|$ and $|V_{\text{VB2,3}}|$ are likely to be higher.

V. DISCUSSION AND CONCLUSIONS

The values for $k_B T_{e,h}$ and $N_{e,h}$ in Figs. 4(a) and 4(b) were obtained by solving Eqs. (11) and (12) assuming that the band gap is renormalized by $|\Delta E^{ee}_{\text{res,ext}}|+|\Delta E^{\text{qs}}_{\text{res,ext}}|$, where $|\Delta E^{\text{qs}}_{\text{res,ext}}|=|V_{C/V,k\cong A}||U_{\text{qs}}|$. To account for possible different values of band gap renormalization between the main VB3 and CB1 bands, we also calculated $k_B T_{e,h}$ and $N_{e,h}$ using two extreme band gap renormalization values: a minimum value of zero (no band gap renormalization) and a maximum value of $|\Delta E^{ee}_{\text{res}}|+|\Delta E^{\text{qs}}_{\text{res}}|$, where $|\Delta E^{\text{qs}}_{\text{res}}|=|V_{C/V,k}||U_{\text{qs}}|$. The latter value is a maximum because $|V_{C/V,k}|$ is the maximum deformation potential we obtained in Sec. IV B, exceeding both $|V_{C/V,k-A}|$ and $|V_{C/V,k\cong A}|$ by a considerable amount. The error bars in Figs. 4(a) and 4(b) reflect these extreme values for $k_B T_{e,h}$ and $N_{e,h}$ and show that the dependence of $k_B T_{e,h}$ and $N_{e,h}$ on the transient band gap renormalization is relatively small. For this reason we used the values reported in Figs. 4(a) and 4(b) throughout this work to calculate the optical deformation potentials for α-Te.

The maximum effective intraband optical deformation potential $|V_{C/V,k}|=2.2\pm0.3$ eV/Å provides a reasonable estimate for the total band gap renormalization in α-Te (Te-I) during a Peierls-like EHP-driven structural transformation to a high-pressure metallic phase. Such transformations may occur when the A_1-type displacement reaches certain critical values. For example, a transition to a Te-III phase with a rhombohedral[13] or orthorhombic[24] structure is expected for an ionic displacement $U_{\text{str,III}}\approx 0.3$ Å ($x=\frac{1}{3}$, where x is the internal structural parameter of α-Te, representing a fraction of the inter-helical distance[13]). Likewise, an ionic displacement $U_{\text{str,II}}\approx 1.1$ Å $(x=\frac{1}{2})$ gives rise to a transition to a Te-II phase with a monoclinic structure.[24,29] If we extrapolate the experimental curves in Figs. 5 and 6 to complete softening of the A_1-phonon mode and complete shrinkage of the average direct band gap we obtain a threshold value for the EHP density of 0.05–0.07 N_V or $1-1.4\times10^{22}$ cm^{-3} (see Sec. IV). If we now extrapolate the experimental $U_{\text{qs}}(N_{e,h})$ values in Fig. 7 to the same threshold density $N_{e,h}\approx(N_{\text{BG},k\approx A,k-A},N_{\text{soft,exp}})$, we obtain a critical sublattice displacement $U_{\text{qs}}\approx 1.2$ Å, which is nearly equal to the above mentioned theoretical value of $U_{\text{str,II}}\approx 1.1$ Å. Such a displacement yields a coherent optical phonon-induced band gap renormalization of about 1 eV near the A point and of about 2.5–3 eV for the near-edge CB1 and VB3 subbands, thus closing direct band gaps at most of the high-symmetry points and mixing up the CB1 and VB3 subbands enough to provide the required high degeneracy of the new structural phase.[1,13]

The effective intraband optical deformation potential $|V_{C/V,k}|=2.2\pm0.3$ eV/Å is three times larger than the intraband optical deformation potentials $|V_{C/V,k\cong A}|=0.7\pm0.1$ eV/Å and $|V_{C/V,k-A}|=0.5\pm0.2$ eV/Å. This observation suggests that the most important contributions to $|V_{C/V,k\cong A}|$ and $|V_{C/V,k-A}|$ come from electron (hole) states in low-dispersion regions of CB1 (VB3) bands around the high-symmetry A and Γ points (Fig. 3). In contrast, the main contribution to $|V_{C/V,k}|$ is due to highly populated electron and, especially, hole states at the bottom and top near-edge H point subbands of the CB1 and VB3 bands, respectively. These bands contribute little to the shifts in the absorption peaks at $E_{\text{res,ext}}$ and $E_{\text{res,ord}}$ near 2 eV because of the corresponding high subband dispersion and transient band filling effects. Therefore, the high value for the intraband optical deformation potential $|V_{C/V,k}|$ may be attributed to the intraband optical deformation potential of hole states $|V_{V,k}|$ in the H valleys of the two upper VB3 subbands of α-Te. This conclusion is consistent with the observation that the crystalline lattice of α-Te—especially the nearest and second-nearest neighbor distances—is most sensitive to electron density changes in the H valleys.[13] For this reason highly occupied electronic states in the H valleys of near-edge CB1 and VB3 subbands, should exhibit the largest band gap renormalization and drive the coherent A_1-phonon mode.

The values we obtain for the intraband optical deformation potentials $|V_{C/V,k}|$, $|V_{C/V,k\cong A}|$, and $|V_{C/V,k-A}|$ of α-Te are much smaller than those for wide band gap semiconductors, such as Si, Ge, GaAs, and diamond, which are on the order of 10–100 eV/Å.[11] Optical deformation potentials represent a crystalline potential energy change per unit displacement and provide a measure of the lattice displacement per unit electronic excitation [see Eq. (3)]. Therefore, smaller intraband optical deformation potentials in a narrow band gap semiconductor such as α-Te, with weaker covalent bonds and a softer crystalline lattice [$\Omega_{\text{o}}\approx 1-4$ THz (Ref. 11)] support an intuitively obvious fact: these materials are considerably closer to a conducting, higher-symmetry Peierls phase, than wide band gap semiconductors with more rigid lattices [$\Omega_{\text{o}}\approx 7-16$ THz (Ref. 11)], which would require much bigger lattice displacements in order to complete a structural transformation.

No values have been reported to date for the *interband* optical deformation potentials in α-Te. However, the values for $\Omega_{\text{th}}(N_{e,h})$ obtained from DFT calculations (see triangles in Fig. 5)[13] are consistent with the corresponding experimental data we used to determine the interband optical deformation potentials $|V_{\text{CB1,2}}|$ and $|V_{\text{VB2,3}}|$. Furthermore, the intraband and interband optical deformation potentials for α-Te obtained in this work are of the same order of magnitude, as is usually the case for other semiconductors.[10,11,24]

In conclusion, we determined values for the effective intraband and interband optical deformation potentials of α-Te from experimental data on the sub-picosecond shrinking of its band gap and the softening of its fully symmetrical center-zone A_1-phonon mode. The values we obtain are consistent with values obtained from theoretical studies.

ACKNOWLEDGMENTS

The research described in this paper was supported by the National Science Foundation under Grant No. DMR-0303642.

*Present address: MIT Lincoln Laboratories, 244 Wood Street, Lexington, MA 02420, USA.

[1] H. J. Zeiger, J. Vidal, T. K. Cheng, E. P. Ippen, G. Dresselhaus, and M. S. Dresselhaus, Phys. Rev. B **45**, 768 (1992).

[2] S. Hunsche, K. Wienecke, T. Dekorsy, and H. Kurz, Phys. Rev. Lett. **75**, 1815 (1995); S. Hunsche and H. Kurz, Appl. Phys. A **65**, 221 (1997).

[3] A. M.-T. Kim, C. A. D. Roeser, and E. Mazur, Phys. Rev. B **68**, 012301 (2003); C. A. D. Roeser, M. Kandyla, A. Mendioroz, and E. Mazur, *ibid.* **70**, 212302 (2004).

[4] K. Sokolowski-Tinten, C. Blome, J. Blums, A. Cavalleri, C. Dietrich, A. Tarasevitch, I. Uschmann, E. Forster, M. Kammler, M. Horn-von Hoegen, and D. von der Linde, Nature (London) **422**, 287 (2003).

[5] M. Hase, M. Kitajima, S. I. Nakashima, and K. Mizoguchi, Phys. Rev. Lett. **88**, 067401 (2002); U. Bovensiepen, A. Melnikov, I. Radu, O. Krupin, K. Starke, M. Wolf, and E. Matthias, Phys. Rev. B **69**, 235417 (2004); M. Hase, K. Ishioka, J. Demsar, K. Ushida, and M. Kitajima, *ibid.* **71**, 184301 (2005).

[6] H. J. Zeiger, T. K. Cheng, E. P. Ippen, J. Vidal, G. Dresselhaus, and M. S. Dresselhaus, Phys. Rev. B **54**, 105 (1996); M. F. DeCamp, D. A. Reis, P. H. Bucksbaum, and R. Merlin, *ibid.* **64**, 092301 (2001).

[7] C. D. Spataru, L. X. Benedict, and S. G. Louie, Phys. Rev. B **69**, 205204 (2004); see also A. Oschlies, R. W. Godby, and R. J. Needs, *ibid.* **45**, 13741 (1992) and D. H. Kim, H. Ehrenreich, and E. Runge, Solid State Commun. **89**, 119 (1994).

[8] R. E. Peierls, *Quantum Theory of Solids* (Clarendon Press, Oxford, 1955), Chap. 5; R. E. Peierls, *More Surprises in Theoretical Physics* (Princeton University Press, Princeton, 1991), Chap. 2.

[9] E. M. Conwell and M. O. Vassel, IEEE Trans. Electron Devices **13**, 22 (1966); A. Leitenstorfer, S. Hunsche, J. Shah, M. C. Nuss, and W. H. Knox, Phys. Rev. Lett. **82**, 5140 (1999); see also B. K. Ridley, *Quantum Processes in Semiconductors* (Clarendon, Oxford, 1988).

[10] P. Y. Yu and M. Cardona, *Fundamentals of Semiconductors: Physics and Material Properties* (Springer, Berlin, 1999).

[11] F. Cedeira and M. Cardona, Phys. Rev. B **5**, 1440 (1972); M. Cardona, M. Grimsditch, and D. Olego, in *Light Scattering in Solids*, edited by J. L. Birman, H. Z. Cummins, and K. K. Rebane (Plenum, New York, 1979), p. 249.

[12] C. A. D. Roeser, Ph.D. thesis, Harvard University, 2003.

[13] P. Tangney, M.Sc. thesis, University College, Cork, 1998; P. Tangney and S. Fahy, Phys. Rev. Lett. **82**, 4340 (1999); P. Tangney and S. Fahy, Phys. Rev. B **65**, 054302 (2002).

[14] T. Dekorsy, H. Auer, C. Waschke, H. J. Bakker, H. G. Roskos, H. Kurz, V. Wagner, and P. Grosse, Phys. Rev. Lett. **74**, 738 (1995).

[15] A. V. Kuznetsov and C. J. Stanton, Phys. Rev. Lett. **73**, 3243 (1994).

[16] P. L. Taylor, *A Quantum Approach to the Solid State* (Prentice Hall, Englewood Cliffs, 1970).

[17] R. H. Landau, *Quantum Mechanics II* (Wiley, New York, 1990).

[18] C. A. D. Roeser, A. M.-T. Kim, J. P. Callan, L. Huang, E. N. Glezer, Y. Siegal, and E. Mazur, Rev. Sci. Instrum. **74**, 3413 (2003).

[19] S. Backus, J. Peatross, C. P. Huang, M. M. Murnane, and H. C. Kapteyn, Opt. Lett. **20**, 2000 (1995).

[20] T. F. Albrecht, K. Seibert, and H. Kurz, Opt. Commun. **84**, 223 (1991).

[21] S. A. Kovalenko, A. L. Dobryakov, J. Ruthmann, and N. P. Ernsting, Phys. Rev. A **59**, 2369 (1999).

[22] *Handbook of Optical Constants of Solids*, edited by E. D. Palik (Academic Press, San Diego, 1991).

[23] N. W. Ashcroft and N. D. Mermin, *Solid State Physics* (Saunders College, Philadelphia, 1976).

[24] Landolt-Bornstein, *Numerical Data and Functional Relationships in Science and Technology*, New Series, V. III 41, *Semiconductors C: Non-Tetrahedrally Bonded Elements and Binary Compounds I*, edited by O. Madelung (Springer-Verlag, Berlin, 1998).

[25] D. Hulin, M. Combescot, J. Bok, A. Migus, J. Y. Vinet, and A. Antonetti, Phys. Rev. Lett. **52**, 1998 (1984); J. R. Goldman and J. A. Prybyla, *ibid.* **72**, 1364 (1994); R. Buhleier, G. Lüpke, G. Marowsky, Z. Gogolak, and J. Kuhl, Phys. Rev. B **50**, 2425 (1994); K. Sokolowski-Tinten and D. von der Linde, *ibid.* **61**, 2643 (2000); A. V. Kimel, F. Bentivegna, V. N. Gridnev, V. V. Pavlov, R. V. Pisarev, and Th. Rasing, *ibid.* **63**, 235201 (2001); A. J. Sabbah and D. M. Riffe, *ibid.* **66**, 165217 (2002).

[26] Th. Starkloff and J. D. Joannopoulos, Phys. Rev. B **19**, 1077 (1979).

[27] J. I. Pankove, *Optical Processes in Semiconductors* (Dover, New York, 1971).

[28] P. Stampfli and K. H. Bennemann, Phys. Rev. B **49**, 7299 (1994); J. S. Graves and R. E. Allen, *ibid.* **58**, 13627 (1998); V. I. Emel'yanov and D. V. Babak, Phys. Solid State **41**, 1338 (1999).

[29] F. A. Blum, Jr. and B. C. Deaton, Phys. Rev. **137**, A1410 (1965); G. Doerre and J. D. Joannopoulos, Phys. Rev. Lett. **43**, 1040 (1979); G. Parthasarathy and W. B. Holzapfel, Phys. Rev. B **37**, 8499 (1988); F. Kirchhoff, N. Binggeli, G. Galli, and S. Massidda, *ibid.* **50**, 9063 (1994); P. Vulliet and J. P. Sanchez, *ibid.* **58**, 171 (1998); N. Funamori and K. Tsuji, *ibid.* **65**, 014105 (2001); C. Hejny and M. I. McMahon, *ibid.* **70**, 184109 (2004).